Stretching and Controlled Motion of Single-Stranded DNA in Locally Heated Solid-State Nanopores

Maxim Belkin,[†] Christopher Maffeo,[†] David B. Wells,[†] and Aleksei Aksimentiev[†,‡,*]

[†]Department of Physics, and [‡]Beckman Institute for Advanced Science and Technology, University of Illinois at Urbana—Champaign, Urbana, Illinois 61801, United States

ABSTRACT Practical applications of solid-state nanopores for DNA detection and sequencing require the electrophoretic motion of DNA through the nanopores to be precisely controlled. Controlling the motion of single-stranded DNA presents a particular challenge, in part because of the multitude of conformations that a DNA strand can adopt in a nanopore. Through continuum, coarse-grained and atomistic modeling, we demonstrate that local heating of the nanopore volume can be used to alter the electrophoretic mobility and conformation of single-stranded DNA. In the nanopore systems considered, the temperature near the nanopore is modulated *via* a nanometer-size heater element that can be radiatively switched on and off. The local enhancement of temperature produces considerable stretching of the DNA fragment confined within the nanopore. Such stretching is reversible, so that the conformation of DNA can be toggled between compact (local heating is off) and extended (local heating is on) states. The effective thermophoretic force acting on single-stranded DNA in the vicinity of the nanopore is found to be sufficiently large (4—8 pN) to affect such changes in the DNA conformation. The local heating of the nanopore volume is observed to promote single-file translocation of DNA strands at transmembrane biases as low as 10 mV, which opens new avenues for using solid-state nanopores for detection and sequencing of DNA.

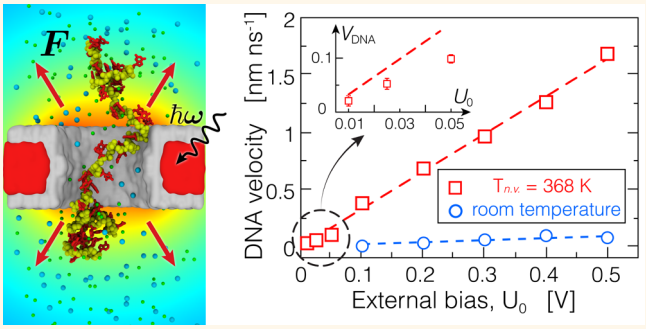

KEYWORDS: thermophoresis · molecular dynamics · nanopores · biosensors · DNA sequencing · molecular separation

Nanopores are remarkable systems that permit sensitive detection of single-molecule events by measuring ionic currents.[1] In a typical nanopore measurement, charged biomolecules dissolved in an electrolyte solution are driven one-by-one through a nanopore in a thin membrane *via* a transmembrane voltage.[2,3] The presence of a single biomolecule in a nanopore modulates the nanopore ionic current, which provides information about the physical and chemical properties of the biomolecule. The nanopore method has been applied to detect and characterize a variety of biomolecules,[4,5] culminating in the detection of the nucleotide sequence of a DNA molecule.[6]

In the case of nanopores made in solid-state membranes, a common problem with performing such measurements is that biomolecules pass through the nanopores too quickly to accurately characterize them *via* ionic current measurement. Various methods have been applied to slow the translocation of biomolecules through nanopores,[7,8] including optical tweezers,[9] magnetic beads,[10] electrostatic[11−14] and steric[15] traps, and modifications to solvent.[16,17] Despite extensive efforts, a general method providing the desired level of control remains a highly researched subject.

Temperature has already been explored as a means to control translocation of DNA through nanopores. The early work of Meller and co-workers demonstrated considerable reduction of the DNA translocation velocity when the temperature of the system containing a biological nanopore α-hemolysin was lowered to 2 °C.[18] A similar method was used to slow translocation of double-stranded DNA and RNA through solid-state nanopores.[19] The α-hemolysin nanopore was engineered to incorporate temperature-sensitive peptides that could open and close the nanopore in response to changing temperature.[20] A temperature-responsive coating was applied to solid-state nanopores to permit modulation of their effective diameters by temperature[21] and,

* Address correspondence to aksiment@illinois.edu.

Received for review April 13, 2013 and accepted July 22, 2013.

Published online July 22, 2013
10.1021/nn403575n

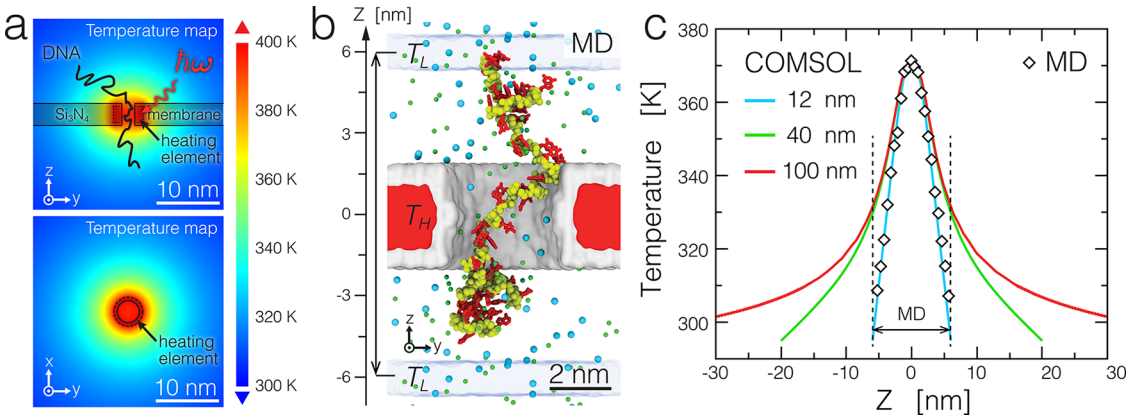

Figure 1. Locally heated solid-state nanopores. (a) Schematics of the system considered. A thin solid-state membrane (semitransparent gray) containing a nanopore is integrated with a heating element (dashed lines) whose temperature is regulated by means of incident radiation (red arrow). Transport and conformation of a single-stranded DNA molecule (black) is regulated by changing the temperature of the heater. The color maps show the steady-state temperature distribution in the system obtained as a solution of continuum heat transfer equations. (b) All-atom model of a locally heated solid-state nanopore. The Si_3N_4 membrane is shown in gray; the heating element in red; the backbone and bases of ssDNA are shown as yellow spheres and red sticks, respectively; K^+ and Cl^- ions as green and blue spheres, respectively; water is not shown. Semitransparent surfaces highlight the volumes kept at 295 K in the dual temperature bath MD simulation. The black arrow indicates the extent of the simulation unit cell. (c) Temperature profiles along the nanopore axis obtained from continuum model and MD simulations. Continuum model data are shown for three cubic systems of different dimensions (solid lines); MD data are shown using symbols. All profiles correspond to the temperature of the heating element of 400 K.

thereby, regulation of the nanopore molecular transport, in particular ionic current.[22−25] Experiments and continuum simulations have shown that Joule heating can create large temperature gradients in micrometer-size pores.[26] Infrared[27] and plasmonic heating[28,29] of the nanopore volume was used to determine the shape of a focused laser beam[28] and to control molecular transport through α-hemolysin.[29] Although discovered more than a century ago, thermophoresis, *i.e.*, the movement of molecules along a temperature gradient, has only recently been applied to control transport in micro and nano systems.[30−33]

In this article, we investigate the effect of local heating on the conformation and electrophoretic mobility of single-stranded DNA. We show that sharp local temperature gradients can produce pronounced stretching of the DNA strand in the vicinity of the nanopore and considerably affect the strand's electrophoretic mobility.

RESULTS AND DISCUSSION

Figure 1a illustrates a solid-state nanopore system considered in this study. The nanopore system is equipped with a local heating element surrounding the nanopore. The heating element can be a thin metallic layer introduced through a combination of atomic layer deposition and electron beam sputtering[28,34,35] or through local modification of the structure of the membrane material.[36] The critical requirement for the material of the element is selective absorption of electromagnetic radiation that can produce rapid local heating. Radiative heating of small metal nanoparticles has been demonstrated in a variety of systems.[28,29,37−41] For gold nanoparticles in water, temperatures exceeding the boiling temperature of water or even the melting temperatures of gold were reported.[42−44] As the heater absorbs radiation, its temperature rises and so does the temperature of the surrounding membrane and solution. However, because the size of the heating element is much smaller than the size of the membrane or solution, the steady-state temperature distribution is highly nonuniform. Figure 1a shows the distribution of the temperature in one such system computed using the COMSOL package.[45] In both media, water and solid-state membrane, temperature drops off as r^{-1}, where r is the distance from the heating element.

To investigate the effect of such local heating on nanopore transport of DNA, we built an all-atom model of a locally heated nanopore system, Figure 1b. In our system, a 54-nucleotide fragment of single-stranded DNA (ssDNA) is threaded halfway through a nanopore in a Si_3N_4 membrane, submerged in 1 M KCl solution. With the use of established protocols of the all-atom molecular dynamics (MD) method,[46] structural and kinetic properties of the system were investigated through a set of simulations lasting several hundreds of nanoseconds each. To model the effect of local heating, the temperature of the membrane interior (atoms located more than 5 Å away from the membrane surface) was controlled independently from the temperature of a 5 Å-thick slab of solution located far from the membrane. When applied, our heating/cooling conditions produce a linear decay of temperature between the heated and cooled regions. Nevertheless, the temperature distributions resulting from our all-atom simulations and from continuum modeling of a much larger system, Figure 1c, are in good agreement in the volume of interest (near the membrane), which justifies the planar heating approximation used in our all-atom simulations. Note that the average temperature inside the

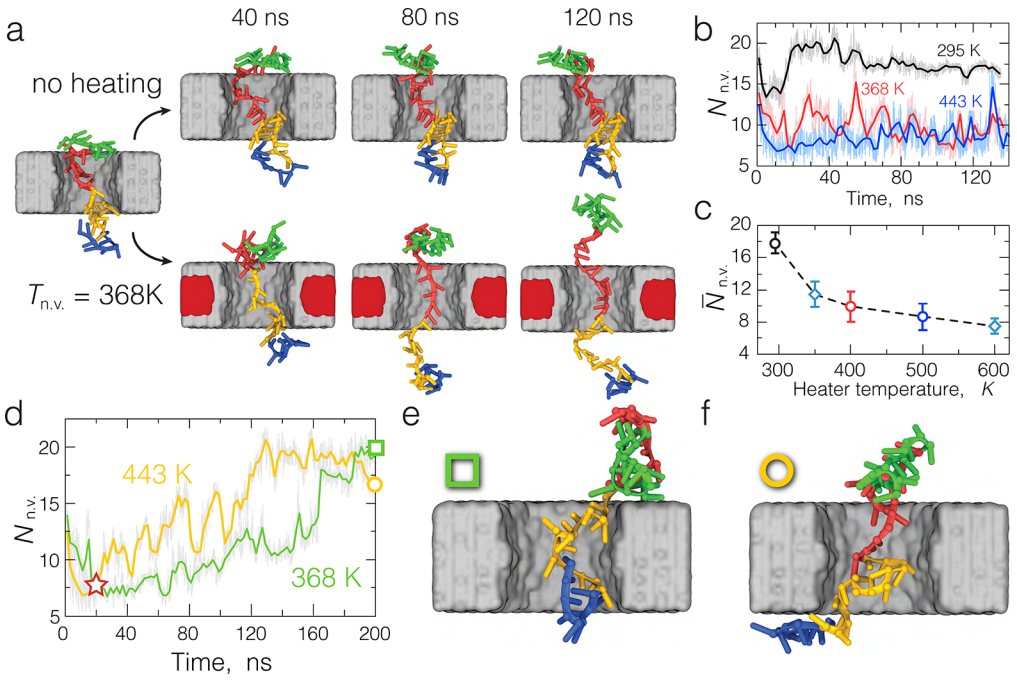

Figure 2. Thermal unwinding of ssDNA in locally heated solid-state nanopores. (a) Snapshots illustrating typical DNA conformations observed in all-atom MD simulations of solid-state nanopores with a uniform temperature of 295 K (top row) and with the temperature of the heating element set to 400 K. In the latter case, the temperature of the solvent in the volume of the nanopore is 368 K. The DNA molecule is shown in balls and sticks representation and colored to reflect its nucleotide sequence (blue adenine, yellow cytosine, red thymine, and green guanine). (b) Number of DNA nucleotides in the nanopore volume, $N_{n.v.}$, *versus* simulation time for several values of the heater element's temperature. Black, red, and blue traces began from the same conformation (shown in panel a) and correspond to the nanopore volume temperatures of 295, 368, and 443 K, respectively (T_H = 295, 400, and 500 K). (c) The average number of nucleotides in the nanopore volume as a function of the heater temperature. (d) Conformational relaxation of ssDNA after the local heating of 400 and 500 K was turned off. The starting points of the relaxation simulations are marked by a star symbol. (e and f) Conformations of DNA at the end of the 200 ns relaxation simulations. Animations M1 and M2 in Supporting Information illustrate typical all-atom MD trajectories of ssDNA unwinding and relaxation.

nanopore volume $T_{n.v.}$ is considerably lower than the temperature of the heating element T_H.

The presence of a temperature gradient was found to produce a considerable change in the conformation of the DNA fragment threaded through the nanopore, Figure 2a. When the system had a uniform room temperature, the DNA fragment maintained its compact structure both inside and outside the nanopore. However, upon assigning the heating element a temperature of 400 K, the fragment of DNA confined in the nanopore visibly straightened. Animation M1 in Supporting Information illustrates this MD trajectory. To quantify the change in the conformation of DNA caused by local heating, the number of nucleotides present in the nanopore volume $N_{n.v.}$ was plotted *versus* time for a set of simulations carried out at several temperatures of the heater, Figure 2b. In all simulations, the DNA reached an unwound state characterized by a low value of $N_{n.v.}$ in less than 20 ns. The average number of DNA nucleotides confined in the nanopore was found to decrease as the temperature of the heating element increased, Figure 2c. In some of the above simulations, the temperature of the nanopore volume exceeded the nominal boiling point of water, but no vapor/liquid segregation was observed within the time and length scales of our MD simulations. These simulations confirmed our conclusions about the effect of temperature gradient on DNA conformation observed at moderate temperatures of the nanopore volume ($T_{n.v}$ < 373 K).

To determine if such a conformational change is reversible, the temperature control of the heating element was switched off after DNA unwinding in the T_H = 400 and 500 K simulations, Figure 2d. In experiment, switching off the heater can be realized by turning off the source of incident radiation. In the simulations, the temperature of the system fell to 295 K within 1 ns. Such rapid cooling is possible because of the nanometer dimensions of the heating element.[47,48] In both simulations, DNA was observed to relax back to conformations typical of room temperature simulations, Figure 2e,f. Animation M2 in Supporting Information illustrates one such trajectory. The 200 ns time scale of conformational relaxation, Figure 2d, is considerably longer than the unwinding and thermalization time scales of 20 and 1 ns, respectively.

The unwinding of ssDNA in locally heated nanopores can result from the elevated temperature of the nanopore volume, the thermophoretic force pulling the two ends of DNA in opposite directions, or the

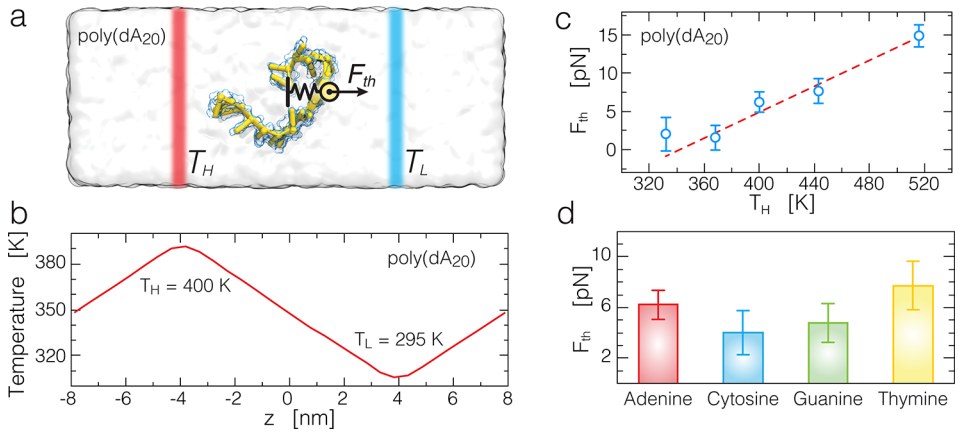

Figure 3. MD simulations of the effective thermophoretic force. (a) Setup of the simulations. A 20-nucleotide DNA homopolymer (poly(dA)$_{20}$ is shown) is placed between two temperature-controlled regions depicted as red and blue stripes. The center of mass of the homopolymer is harmonically restrained to the point equidistant from the highlighted regions. The average displacement of the DNA fragment indicates the effective force of the temperature gradient. (b) Temperature profile along the *z*-axis in the simulations of the effective thermophoretic force. (c) Simulated thermophoretic force *versus* temperature of the hot region T_H; T_L = 295 K in all simulations. (d) Average thermophoretic force for the four DNA homopolymers at T_H = 400 K and T_L = 295 K.

increased electrostatic self-repulsion caused by a change of the electrolyte condition in the nanopore. A plot of Cl^- concentration along the nanopore axis for several values of the nanopore volume temperature, Figure S1, revealed only a moderate decrease of ion concentration, which we assessed as insufficient to produce the observed changes in the DNA conformation.

We elucidated the effect of temperature on the conformation of a DNA strand in the absence of thermophoresis by performing simulations of the ssDNA strand in a uniformly heated 1 M KCl solution. Figure S2a of Supporting Information illustrates a typical simulation system. As in our simulations of the locally heated nanopore systems, ssDNA was observed to change its conformation in bulk solution with temperature: the radius of gyration of ssDNA increased with increasing temperature, Figure S2b. To quantitatively compare the conformations of DNA in the simulations of the nanopore and bulk solution systems, we compared the number of DNA nucleotides located within 17.5 Å of the DNA's center of mass in our bulk solution simulations to the number of DNA nucleotides located within 17.5 Å of the nanopore's center in our simulations of the nanopore systems. The numbers of nucleotides within these regions were found to be in general agreement with one another, Figure S2c, indicating the dominant role of the elevated temperature in the observed unwinding of ssDNA inside the locally heated nanopore systems. This result is not entirely surprising since the temperature variation is small inside the nanopore volume, Figure 1c. At low to moderate temperatures, however, the number of nucleotides in the nanopore system was typically smaller than that in the corresponding bulk solution system, which may indicate the effect of steric confinement that prevented DNA from adopting a spherically symmetric coil conformation.

To evaluate the effect of the thermophoretic force, half of the DNA strand was removed from the nanopore system and the remaining half was moved as a rigid body along the pore axis so that one of its ends coincided with the center of the nanopore. That end of the DNA strand was then harmonically restrained, under the assumption that the product of its mean displacement and the spring constant of the restraining potential would reveal the magnitude of the effective force of the thermal gradient. Unfortunately, significant fluctuations of the force due to interaction of the DNA with the nanopore surface prevented us from drawing any quantitative conclusions about the magnitude of the thermophoretic force within the time scale of our all-atom MD simulations.

We instead measured the magnitude of the thermophoretic force using a simulation system shown in Figure 3a. Displacement of a 20-nucleotide homopolymer harmonically restrained to a point equidistant from the regions of high and low temperature revealed the magnitude and direction of the thermophoretic force. Figure 3b illustrates a typical profile of temperature attained in these simulations. For each of the four DNA homopolymer sequences tested, the thermophoretic force was found to push the DNA strand from the region of high temperature toward the region of low temperature. The magnitude of the force was found to scale linearly with the temperature gradient, Figure 3c. The magnitude of the thermophoretic force experienced by a 20-nucleotide fragment at a 100 K difference over 8 nm was approximately 6 pN, or 0.3 pN per nucleotide. Within the statistical error of our computational experiments, all four DNA homopolymers experienced approximately the same thermophoretic force at the same temperature gradient.

The results of the above simulations suggest that the thermophoretic force alone can have a considerable

effect on the conformation of DNA fragments located in the immediate vicinity of the heating element outside the nanopore, producing pronounced stretching. To demonstrate such an effect, we carried out coarse-grained (CG) MD simulations of a long (125−1000 nucleotides) DNA strand with one end tethered to the center of the nanopore *via* a harmonic potential; the CG model is described in Supporting Information. Figure 4a,b illustrates typical conformations of an ssDNA strand in the CG MD simulations with the local heating source turned off and on. The local heating produces considerable stretching of the DNA strand in the vicinity of the nanopore. Figure 4c shows the average force applied to the tethered end of the DNA as a function of the heater temperature and the length of the DNA strand. The effective thermophoretic force was found to linearly increase with the temperature of the heater, reaching 8 pN for a 100 K difference between the temperature of the heater and the temperature of bulk water 100 nm away from the heater. Even in the latter case, the actual temperature of the solvent within the nanopore remains below the boiling point, Figure 1c. Forces in the 1−10 pN range can produce considerable stretching of ssDNA[49,50] confined within the nanopore.

To determine the effect of local heating on the process of electrophoretically driven DNA translocation, we performed all-atom simulations of locally heated nanopore systems under several transmembrane bias conditions. Our solid-state nanopore systems were subject to a transmembrane electric potential that switched direction every 5 ns, Figure 5a. In the simulations performed at room temperature, displacement of the ssDNA molecule during each 5 ns half-cycle did not exceed 0.5 nm for the transmembrane biases in the 100−300 mV range, Figure 5b. Setting the temperature of the heating element to 400 K considerably increased the amplitude of ssDNA displacement through the nanopore, Figure 5b. Furthermore, stretching of the DNA strand in the locally heated nanopore allowed us to induce oscillatory motion of the strand at low transmembrane biases of 50, 25, and 10 mV (see Supporting Information Figure S4). The average velocity of DNA translocation extracted from the trajectories obtained under the alternating field conditions are shown in Figure 5c. By utilizing local heating, the electrophoretic mobility of ssDNA could be increased by a factor of 20. As such, a large increase in DNA mobility cannot be explained only by the reduced viscosity of the solution (see Supporting Information Figure S5), and we associate the increased mobility with changes in the DNA conformation.

Thus, our results suggest the possibility of controlling the electrophoretic transport of ssDNA through a solid-state nanopore by radiatively switching on and off the local heating element surrounding the nanopore. To determine conditions for exercising such a

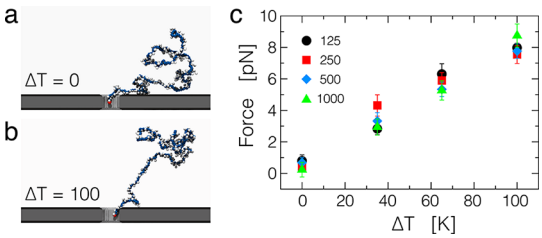

Figure 4. CG MD simulations of ssDNA in a nanopore subject to local heating. (a and b) Representative conformation of a 250-nucleotide ssDNA after 0.8 μs of CG MD simulation of a solid-state nanopore system without any local heating (a) and with the heater temperature set 100 K higher than the solvent temperature (b). The membrane containing the nanopore is shown as a cutaway molecular surface; the DNA is shown as blue and white spheres representing the backbone and base beads of the CG model, respectively (see Supporting Information for a detailed description of the CG model). One terminal bead of the DNA strand (red sphere) is tethered to the plane in the middle of the membrane by means of a harmonic potential. Displacement of the terminal bead along the pore axis reports the effective force experienced by the DNA strand. (c) The average effective force experienced by the bead tethered in the center of the nanopore during CG MD simulations of ssDNA fragments of different length. In this figure, ΔT refers to the difference between the temperature of the heater and the temperature of solution 100 nm away from the heater. Figure 1 illustrates a typical distribution of temperature in these systems.

control, we first investigated the electrophoretic mobility of ssDNA during the on/off cycle of the heater. For our "off" state, we chose the following three DNA conformations: the initial room-temperature conformation shown in Figure 2a, and the two conformations attained by the DNA strand at the end of the relaxation trajectories, Figure 2e,f. As representative conformations for the "on" state, we chose steady-state conformations from two independent trajectories at T_H= 400 and 500 K. Each system was simulated under a 100 mV transmembrane bias at the corresponding temperature of the heating element (295, 400, or 500 K) for 20 or 40 ns. The resulting electrophoretic mobility of DNA as a function of the heater temperature is shown in Figure 5d. Consistent with the results of the alternating electric field simulations, DNA mobility was found to strongly depend on the temperature of the heating element.

In the final set of simulations, we attempted to control DNA transport by switching the local heating on and off while maintaining a constant transmembrane bias. We found the force driving the relaxation of ssDNA from unwound (high mobility) to compact (low mobility) conformations to be considerably smaller than the electrophoretic force driving DNA translocation, which prevented ssDNA from reaching the compact state and, thereby, attaining a lower electrophoretic mobility. Thus, to use local heating as a means of controlling DNA transport, the local temperature must be switched off at the same time or after the transmembrane bias is switched off. Upon relaxation of the DNA conformation

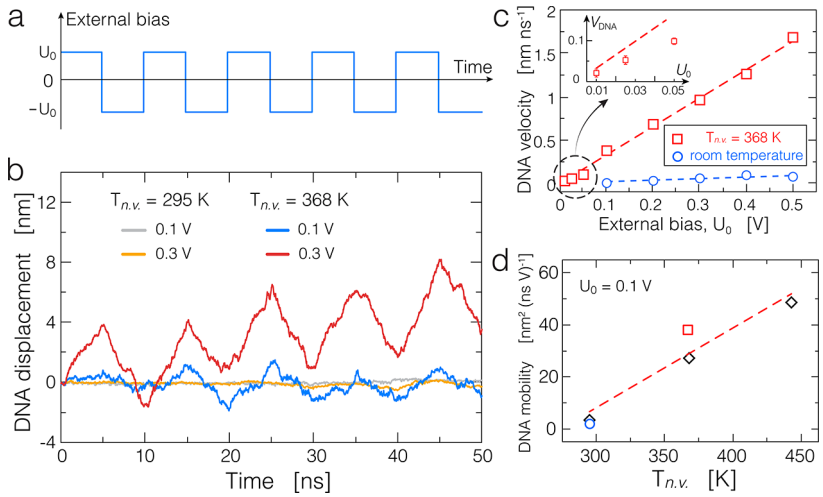

Figure 5. Electrophoretic motion of DNA through a nanopore assisted by local heating. (a) Profile of the transmembrane bias applied in the alternating electric field simulations. (b) DNA translocation driven by alternating electric field. Shown is displacement of ssDNA through the nanopore in MD simulations performed at uniform room temperature and when the temperature of the heater element is set to 400 K (the temperature of the nanopore volume $T_{n.v.}$ = 368 K). (c) Translocation velocity of ssDNA as a function of the transmembrane bias extracted from the simulations of the two nanopore systems under alternating electric field. Lines show linear fits to the data producing the following estimates of the electrophoretic mobility: $\mu_{295\ K}$ = 2.0 nm^2/(ns·V), and $\mu_{368\ K}$ = 38.4 nm^2/(ns·V). The inset shows a close up view of the $U_0 \leq 55$ mV region of the main plot. (d) Electrophoretic mobility of ssDNA *versus* temperature of the nanopore volume, $T_{n.v.}$. Dashed line indicates a linear fit to the data; the slope is 0.3 nm^2/(ns·V·K).

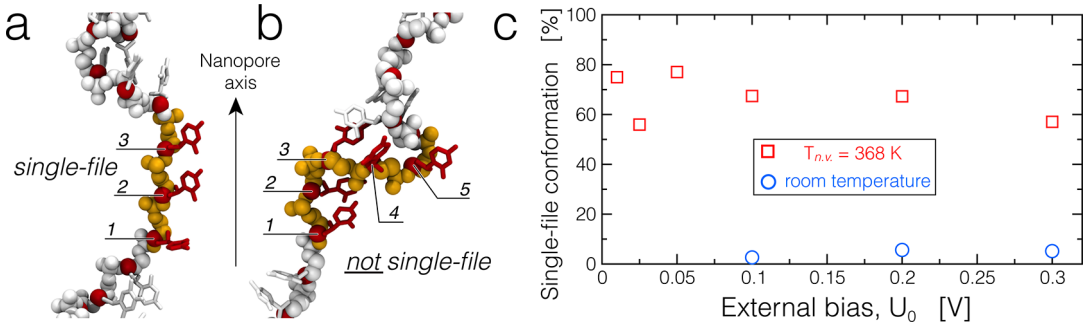

Figure 6. Local heating promotes single-file translocation of ssDNA. (a and b) Example of DNA conformations. (c) The probability of finding a DNA strand in a single-file conformation during all-atom MD simulations of the nanopore system under the alternating transmembrane bias conditions. Local heating dramatically increases the probability of single-file translocation. The overall displacement of the strand is characterized in Figures 5 and S4.

to a compact state, the transmembrane bias can be switched back on to transport DNA at a reduced rate.

Figure 6 details the effect of local heating on the conformation of a single DNA strand in a nanopore. In our analysis, we were primarily interested in determining whether local heating can induce single-file conformations of the DNA strand, which is desirable for DNA sequencing applications. Figure 6a,b shows examples of DNA conformations characterized as (panel a) and not characterized as (panel b) single-file; the detailed description of our analysis procedure is provided in Supporting Information. Figure 6c plots the percentage of single-file conformations observed in the all-atom simulations of the nanopore system under the alternating transmembrane bias conditions. Local heating is seen to dramatically increase the probability of single-file conformations, which can reach 80% even at a very low transmembrane bias (50 mV).

CONCLUSIONS

The ideal scenario for DNA sequencing using a nanopore is slow, unidirectional and single-file translocation of DNA. We have shown that by locally heating the nanopore we can stretch single-stranded DNA to ensure single-file translocation. At the same time, we found that local heating considerably increases the translocation velocity of DNA. The stretching, however, permits realizing single-file translocations even at very low transmembrane biases (10−25 mV). Hence, translocation velocities similar to those observed without local heating could be achieved while having the additional benefits of single-file transport. The thermophoretic stretching of DNA can be instrumental for the realization of electrostatic control over DNA motion in the so-called DNA transistor.[12]

The translocation velocity of 1 nucleotide per 10 ns and the relatively large pore sizes make the systems

considered in this work unsuitable for sequencing DNA by measuring the nanopore ionic current. However, stretching of single-stranded DNA by a local temperature gradient can considerably aid DNA sequence detection in approaches that rely on transverse tunneling current[51] for nucleotide identification. Experimentally, such systems are typically realized using narrow gaps.[52,53] The slit-like geometry of the gap makes folded entry and translocation of a single DNA strand very likely, so an additional system must be designed to ensure single-file translocation. The results of our study suggest that local heating of the nanogap volume can prevent folded translocation of single-stranded DNA. The themophoretic stretching of the DNA strand will also considerably reduce the conformational noise in the tunneling current recording, which can outweigh a higher level of the electronic noise associated with the local heating. Furthermore, the transverse electric field applied to produce the tunneling current can considerably retard stochastic displacement of DNA through the nanopore,[51] in particular at a very low (10−50 mV) transmembrane bias.

In summary, we have determined the behavior of single-stranded DNA molecules in a solid-state nanopore equipped with a local heating element. We found that local heating promotes straightening of the DNA fragment threaded through the nanopore, which is desirable for DNA sequencing applications. The thermophoretic forces were found to be too weak to counter the electrophoretic force of the transmembrane bias but large enough to alter the conformation of a DNA molecule beyond the nanopore. Our results indicate that local heating can be employed to regulate the velocity of ssDNA transport through solid-state nanopores. Possible practical applications of locally heated solid-state nanopores include detection of protein binding to DNA, protein folding-unfolding transition, DNA sequencing and drug design.

METHODS

Continuum Model. Our continuum model of a heated solid-state nanopore system was built using the COMSOL software package. A cylindrical pore of 3.5 nm diameter was made in a 3.5 nm-thick membrane. The properties of the membrane material were set to match the properties of silicon nitride: heat capacity $c_p^m = 710$ J (kg·K)$^{-1}$, density $\rho^m = 3310$ kg·m^{-3}, and thermal conductivity $k^m = 2$ W (m·K)$^{-1}$. The membrane was surrounded by water, $c_p^w = 4181.3$ J (kg·K)$^{-1}$, $\rho^w = 1000$ kg·m^{-3}, and $k^w = 0.58$ W (m·K)$^{-1}$. The entire simulation domain was a cube 12, 40, or 100 nm on a side. The heating element was modeled as a cylindrical ring concentric with the nanopore. The inner surface of the ring had the same diameter as the nanopore, and the outer diameter was 4.5 nm. The height of the heating element was 1 nm; the heating element was located in the middle of the membrane. The temperature of the heating element was set to T_H; Dirichlet boundary conditions ($T = 295$ K) were applied at all sides of the simulations domain. After building the standard mesh, a steady-state solution to the system of coupled heat transfer equations for fluid and solid was obtained using GMRES solver and damped Newton's method in the COMSOL 4.3 software package (Heat Transfer module).[45]

General All-Atom MD Methods. All atomistic MD simulations were performed using the program NAMD2,[54] periodic boundary conditions, the CHARMM27 parameter set for water, ions and nucleic acids,[55] CHARMM-compatible parameters for silicon nitride,[56] and ion-pair specific corrections to the Lennard-Jones parameter σ.[57] All simulations employed 2−2−6-fs multiple timestepping, SETTLE algorithm to keep water molecules rigid,[58] RATTLE algorithm to keep rigid all other covalent bonds involving hydrogen atoms,[59] a 7−8 Å cutoff for van der Waals and short-range electrostatic forces. Long-range electrostatic interactions were computed using the particle mesh Ewald method[60] over a 1.0 Å resolution grid with the net momentum removed before every full electrostatics calculation (zeroMomentum feature of NAMD2).[61]

All-Atom Model of the Solid-State Nanopore−DNA System. An all-atom model of a 3.5 nm-thick Si_3N_4 membrane was built according to procedures described elsewhere.[56] A double-cone pore of a 3.5 nm-diameter in its center and 4.3 nm-diameter openings at both sides was cut by removing atoms from the membrane. A 54-nucleotide 5′-(dA)$_9$-(dC)$_{15}$-(dT)$_{15}$-(dG)$_{15}$-3′ DNA strand was threaded halfway through the nanopore. The system was then solvated using the Solvate plugin of VMD.[62] Following that, the system was neutralized by adding K^+ and Cl^- ions in the amounts necessary to produce a 1 M solution. The final system was a 117 Å-long hexagonal prism with a side of 79 Å; hexagonal periodic boundary conditions were applied in the *xy*-plane. In all simulations of the Si_3N_4 systems, atoms of the membrane were harmonically restrained to their initial coordinates. The spring constant of the harmonic constraints applied to the surface or bulk atoms of the membrane was 10 or 1 kcal/(mol·Å^2), respectively. To reduce adhesion of DNA to the nanopore surface, a custom potential[56] was applied to DNA atoms by means of the GridForce feature of NAMD2.[63]

Each system underwent 4000 steps of energy minimization using the conjugate gradient method before being equilibrated for 6 ns in the NPT ensemble, *i.e.*, constant number of particles *N*, pressure *P* and temperature *T*. During this equilibration, a Langevin thermostat[64] with a damping coefficient of 0.02 ps^{-1} kept the temperature at 295 K; Nosé-Hoover Langevin piston pressure control[65] was used to maintain the pressure at 1 atm by adjusting the system's dimension normal to the plane of the Si_3N_4 membrane. The mean length of the system during the last 4 ns of the NPT equilibration was used in all production simulations.

In our simulations of electric field-driven transport of DNA through the nanopores, an external electric field was applied in the direction normal to the membrane (along the *z* axis). The external fields are reported in terms of a transmembrane voltage difference $V = -EL_z$, where E is the electric field strength and L_z is the length of the simulation system in the *z* direction.[66]

MD Simulations of the Effective Thermophoretic force. The effective force of a temperature gradient on a DNA fragment was measured using four simulation systems each containing a poly(dA)$_{20}$, poly(dC)$_{20}$, poly(dG)$_{20}$ or poly(dT)$_{20}$ fragment of ssDNA submerged in 1 M KCl solution approximately 60 × 60 × 160 Å^3 in volume. Following energy minimization, each system was equilibrated for 6 ns in the NPT ensemble to obtain the average dimensions of the system. The DNA molecule was initially placed equidistant from the two different-temperature thermostat regions, which were 5-Å-wide rectangular slabs, Figure 3a. Room temperature (295 K) was maintained in one of the slab regions. The temperature of the other region was set to a higher value (T_H), producing a stationary temperature gradient between the slabs. The steered molecular dynamics (SMD) protocol[67] was used to restrain the center of mass of the DNA fragment. The motion of the DNA fragment was restrained only in the direction normal to the thermostat regions (along the *z*-axis); the DNA could freely move parallel to the slabs. The SMD spring constant of $k_z = 0.29$ kcal/(mol·Å^2) was used, which corresponds to the force of ~20 pN for a displacement of $dz = 1$ Å.

During the course of a constant volume simulation, displacement of the center of mass of the DNA fragment was recorded every 9.6 ps and was used to determine the effective force experienced by the fragment as $F_{eff}(t) = k_z \cdot dz(t)$. The average force was determined by averaging the instantaneous force values over the entire trajectory. The poly(dA)$_{20}$ system was simulated at several temperature gradients corresponding to $T_H = 350$, 400, and 500 K. All other homopolymers were simulated for only one temperature gradient corresponding to $T_H = 400$ K. Systems containing poly(dC)$_{20}$, poly(dG)$_{20}$ and poly(dT)$_{20}$ fragments were simulated for 80 ns, whereas simulations of the poly(dA)$_{20}$ system lasted ~170 ns each.

Dual Thermal Bath Simulations of All-Atom Systems. Two thermal baths were used to produce a stationary temperature gradient in our all-atom systems. In the case of Si_3N_4 nanopore systems, the temperature gradient was established between the heated membrane and a slab of cooled water. The temperature of the membrane was controlled by the Langevin thermostat applied to the membrane atoms located 5 Å away from the nanopore surface. At the same time, the Lowe-Andersen[68] thermostat was applied to water molecules confined inside a 5-Å-wide slab. The slab was arranged parallel to the membrane and positioned such that under the periodic boundary conditions two equal-magnitude opposite-direction temperature gradients were formed on both sides of the membrane, as in Figure 1b of the main text. Importantly, our custom implementation of the Lowe-Andersen thermostats allowed us to control the temperature of a specified volume inside our simulation system. Water, ions and DNA could freely enter and exit the volume subject to the Lowe-Andersen thermostat, whereas the Langevin thermostat was applied to a fixed set of membrane atoms independent of their position.

In our simulations of the effective thermophoretic force in bulk solution, two Lowe-Andersen thermostats were employed, each confined to one of two 5-Å-wide slabs arranged parallel to each other. The location of the slabs was chosen such that two equal-magnitude opposite-direction temperature gradients were produced between the slabs under the periodic boundary conditions.

Our dual temperature bath simulations were performed using a custom version of NAMD2. The GridForce feature[63] of NAMD2 was used to define regions in the system where individual Lowe-Andersen thermostats were applied to select sets of atoms.

Conflict of Interest: The authors declare no competing financial interest.

Acknowledgment. This work was supported by the grants from the National Science Foundation (DMR-0955959 and PHY-0822613), the National Institutes of Health (R01-HG005115) and through a cooperative research agreement with the Oxford Nanopore Technologies. The authors gladly acknowledge supercomputer time provided through XSEDE Allocation Grant MCA05S028 and the Taub Cluster (UIUC). A.A. would like to thank the Department of Bionanosciences at the Delft University of Technology for hospitality and support from The Netherlands Organisation for Scientific Research (NWO).

Supporting Information Available: Detailed description of the CG model and its application to the simulation of locally heated nanopore systems, detailed description of the analysis methods; plots of the local ion concentration profiles, the radius of gyration in bulk solution, validation of the CG model, DNA displacements at low transmembrane biases, and the dependence of solvent viscosity on temperature; animations illustrating typical simulation trajectories. This material is available free of charge *via* the Internet at http://pubs.acs.org.

REFERENCES AND NOTES

1. Dekker, C. Solid-State Nanopores. *Nat. Nanotechnol.* **2007**, *2*, 209–215.
2. Bezrukov, S. M.; Vodyanoy, I.; Parsegian, V. A. Counting Polymers Moving through a Single Ion Channel. *Nature* **1994**, *370*, 279–281.
3. Kasianowicz, J. J.; Brandin, E.; Branton, D.; Deamer, D. W. Characterization of Individual Polynucleotide Molecules Using a Membrane Channel. *Proc. Natl. Acad. Sci. U.S.A.* **1996**, *93*, 13770–13773.
4. Kasianowicz, J.; Robertson, J. W. F.; Chan, E. R.; Reiner, J. E.; Stanford, V. M. Nanoscopic Porous Sensors. *Annu. Rev. Anal. Chem.* **2008**, *1*, 737–766.
5. Howorka, S.; Siwy, Z. Nanopore Analytics: Sensing of Single Molecules. *Chem. Soc. Rev.* **2009**, *38*, 2360–2384.
6. Manrao, E. A.; Derrington, I. M.; Laszlo, A. H.; Langford, K. W.; Hopper, M. K.; Gillgren, N.; Pavlenok, M.; Niederweis, M.; Gundlach, J. H. Reading DNA at Single-Nucleotide Resolution with a Mutant MspA Nanopore and Phi29 DNA Polymerase. *Nat. Biotechnol.* **2012**, *30*, 349–353.
7. Keyser, U. F. Controlling Molecular Transport through Nanopores. *J. R. Soc., Interface* **2011**, *8*, 1369–1378.
8. Luan, B.; Stolovitzky, G.; Martyna, G. Slowing and Controlling the Translocation of DNA in a Solid-State Nanopore. *Nanoscale* **2012**, *4*, 1068–1077.
9. Keyser, U.; Koeleman, B.; Dorp, S.; Krapf, D.; Smeets, R.; Lemay, S.; Dekker, N.; Dekker, C. Direct Force Measurements on DNA in a Solid-State Nanopore. *Nat. Phys.* **2006**, *2*, 473–477.
10. Peng, H.; Ling, X. S. Reverse DNA Translocation through a Solid-State Nanopore by Magnetic Tweezers. *Nanotechnology* **2009**, *20*, 185101.
11. Melnikov, D. V.; Leburton, J.-P.; Gracheva, M. E. Slowing Down and Stretching DNA with an Electrically Tunable Nanopore in a p−n Semiconductor Membrane. *Nanotechnology* **2012**, *23*, 255501.
12. Polonsky, S.; Rossnagel, S.; Stolovitzky, G. Nanopore in Metal-Dielectric Sandwich for DNA Position Control. *Appl. Phys. Lett.* **2007**, *91*, 153103.
13. Luan, B.; Peng, H.; Polonsky, S.; Rossnagel, S.; Stolovitzky, G.; Martyna, G. Base-By-Base Ratcheting of Single Stranded DNA through a Solid-State Nanopore. *Phys. Rev. Lett.* **2010**, *104*, 238103.
14. Tsutsui, M.; He, Y.; Furuhashi, M.; Rahong, S.; Taniguchi, M.; Kawai, T. Transverse Electric Field Dragging of DNA in a Nanochannel. *Sci. Rep.* **2012**, *2*, 394.
15. Mirsaidov, U.; Comer, J.; Dimitrov, V.; Aksimentiev, A.; Timp, G. Slowing the Translocation of Double-Stranded DNA Using a Nanopore Smaller than the Double Helix. *Nanotechnology* **2010**, *21*, 395501.
16. Fologea, D.; Uplinger, J.; Thomas, B.; McNabb, D. S.; Li, J. Slowing DNA Translocation in a Solid-State Nanopore. *Nano Lett.* **2005**, *5*, 1734–1737.
17. Kowalczyk, S. W.; Wells, D. B.; Aksimentiev, A.; Dekker, C. Slowing Down DNA Translocation through a Nanopore in Lithium Chloride. *Nano Lett.* **2012**, *12*, 1038–1044.
18. Meller, A.; Nivon, L.; Branton, D. Voltage-Driven DNA Translocations through a Nanopore. *Phys. Rev. Lett.* **2001**, *86*, 3435–3438.
19. Wanunu, M.; Morrison, W.; Rabin, Y.; Grosberg, A. Y.; Meller, A. Electrostatic Focusing of Unlabelled DNA Into Nanoscale Pores Using a Salt Gradient. *Nat. Nanotechnol.* **2010**, *5*, 160–165.
20. Jung, Y.; Bayley, H.; Movileanu, L. Temperature-Responsive Protein Pores. *J. Am. Chem. Soc.* **2006**, *128*, 15332–15340.
21. Reber, N.; Kuchel, A.; Spohr, R.; Wolf, A.; Yoshida, M. Transport Properties of Thermo-Responsive Ion Track Membranes. *J. Membr. Sci.* **2001**, *193*, 49–58.
22. Schepelina, O.; Zharov, I. PNIPAAM-Modified Nanoporous Colloidal Films with Positive and Negative Temperature Gating. *Langmuir* **2007**, *23*, 12704–12709.
23. Yameen, B.; Ali, M.; Neumann, R.; Ensinger, W.; Knoll, W.; Azzaroni, O. Ionic Transport through Single Solid-State Nanopores Controlled with Thermally Nanoactuated Macromolecular Gates. *Small* **2009**, *5*, 1287–1291.
24. Guo, W.; Xia, H.; Xia, F.; Hou, X.; Cao, L.; Wang, L.; Xue, J.; Zhang, G.; Song, Y.; Zhu, D.; *et al.* Current Rectification in Temperature-Responsive Single Nanopores. *ChemPhysChem* **2010**, *11*, 859–864.
25. Nasir, S.; Ali, M.; Ensinger, W. Thermally Controlled Permeation of Ionic Molecules through Synthetic Nanopores Functionalized with Amine-Terminated Polymer Brushes. *Nanotechnology* **2012**, *23*, 225502.
26. Viasnoff, V.; Bockelmann, U.; Meller, A.; Isambert, H.; Laufer, L.; Tsori, Y. Localized Joule Heating Produced by Ion

Current Focusing through Micron-Size Holes. *Appl. Phys. Lett.* **2010**, *96*, 163701.
27. Keyser, U. F.; Krapf, D.; Koeleman, B. N.; Smeets, R. M. M.; Dekker, N. H.; Dekker, C. Nanopore Tomography of a Laser Focus. *Nano Lett.* **2005**, *5*, 2253–2256.
28. Jonsson, M. P.; Dekker, C. Plasmonic Nanopore for Electrical Profiling of Optical Intensity Landscapes. *Nano Lett.* **2013**, *13*, 1029–1033.
29. Reiner, J. E.; Robertson, J. W. F.; Burden, D. L.; Burden, L. K.; Balijepalli, A.; Kasianowicz, J. J. Temperature Sculpting in Yoctoliter Volumes. *J. Am. Chem. Soc.* **2013**, *135*, 3087–3094.
30. Mast, C. B.; Braun, D. Thermal Trap for DNA Replication. *Phys. Rev. Lett.* **2010**, *104*, 188102.
31. Duhr, S.; Braun, D. Optothermal Molecule Trapping by Opposing Fluid Flow with Thermophoretic Drift. *Phys. Rev. Lett.* **2006**, *97*, 038103.
32. Jerabek-Willemsen, M.; Wienken, C. J.; Braun, D.; Baaske, P.; Duhr, S. Molecular Interaction Studies Using Microscale Thermophoresis. *Assay Drug Dev. Technol.* **2011**, *9*, 342–353.
33. He, Y.; Tsutsui, M.; Scheicher, R. H.; Bai, F.; Taniguchi, M.; Kawai, T. Thermophoretic Manipulation of DNA Translocation through Nanopores. *ACS Nano* **2013**, *7*, 538–546.
34. Healy, K.; Schiedt, B.; Morrison, A. P. Solid-State Nanopore Technologies for Nanopore-Based DNA Analysis. *Nanomedicine* **2007**, *2*, 875–897.
35. Miles, B. N.; Ivanov, A. P.; Wilson, K. A.; Dogan, F.; Japrung, D.; Edel, J. B. Single Molecule Sensing with Solid-State Nanopores: Novel Materials, Methods, and Applications. *Chem. Soc. Rev.* **2013**, *42*, 15–28.
36. Venkatesan, B. M.; Shah, A. B.; Zuo, J.-M.; Bashir, R. DNA Sensing Using Nanocrystalline Surface-Enhanced Al2O3 Nanopore Sensors. *Adv. Funct. Mater.* **2010**, *20*, 1266–1275.
37. Tjahjono, I. K.; Bayazitoglu, Y. Near-Infrared Light Heating of a Slab by Embedded Nanoparticles. *Int. J. Heat Mass Transfer* **2008**, *51*, 1505–1515.
38. Harata, A.; Shen, Q.; Sawada, T. Photothermal Applications of Lasers: Study of Fast and Ultrafast Photothermal Phenomena at Metal-Liquid Interfaces. *Annu. Rev. Phys. Chem.* **1999**, *50*, 193–219.
39. Hanson, G. W.; Patch, S. K. Optimum Electromagnetic Heating of Nanoparticle Thermal Contrast Agents at RF Frequencies. *J. Appl. Phys.* **2009**, 106.
40. Roder, P. B.; Pauzauskie, P. J.; Davis, E. J. Nanowire Heating by Optical Electromagnetic Irradiation. *Langmuir* **2012**, *28*, 16177–16185.
41. Baffou, G.; Rigneault, H. Femtosecond-Pulsed Optical Heating of Gold Nanoparticles. *Phys. Rev. B* **2011**, *84*.
42. Hu, M.; Petrova, H.; Hartland, G. V. Investigation of the Properties of Gold Nanoparticles in Aqueous Solution at Extremely High Lattice Temperatures. *Chem. Phys. Lett.* **2004**, *391*, 220–225.
43. Plech, A.; Kotaidis, V.; Grésillon, S.; Dahmen, C.; von Plessen, G. Laser-Induced Heating and Melting of Gold Nanoparticles Studied by Time-Resolved X-ray Scattering. *Phys. Rev. B* **2004**, *70*, 195423.
44. Kotaidis, V.; Dahmen, C.; von Plessen, G.; Springer, F.; Plech, A. Excitation of Nanoscale Vapor Bubbles at the Surface of Gold Nanoparticles in Water. *J. Chem. Phys.* **2006**, *124*, 184702.
45. Pryor, R. *Multiphysics Modeling Using COMSOL 4: A First Principles Approach*; Mercury Learning Series; Mercury Learning & Information: Dulles, VA, 2012.
46. Aksimentiev, A. Deciphering Ionic Current Signatures of DNA Transport through a Nanopore. *Nanoscale* **2010**, *2*, 468–483.
47. Pelesko, J.; Bernstein, D. *Modeling MEMS and NEMS*; CRC Press LLC: Boca Raton, FL, 2002.
48. Merabia, S.; Shenogin, S.; Joly, L.; Keblinski, P.; Barrat, J.-L. Heat Transfer From Nanoparticles: A Corresponding State Analysis. *Proc. Natl. Acad. Sci. U.S.A.* **2009**, *106*, 15113–15118.
49. Seol, Y.; Skinner, G. M.; Visscher, K. Stretching of Homopolymeric RNA Reveals Single-Strand Helices and Base-Stacking. *Phys. Rev. Lett.* **2007**, *98*, 158103–158106.
50. Ke, C.; Jiang, Y.; Rivera, M.; Clark, R. L.; Marszalek, P. E. Pulling Geometry Induced Errors in Single Molecule Force Spectroscopy Measurements. *Biophys. J.* **2007**, *92*, 76–78.
51. Lagerqvist, J.; Zwolak, M.; Ventra, M. D. Fast DNA Sequencing *via* Transverse Electronic Transport. *Nano Lett.* **2006**, *6*, 779–782.
52. Huang, S.; He, J.; Chang, S.; Zhang, P.; Liang, F.; Li, S.; Tuchband, M.; Fuhrmann, A.; Ros, R.; Lindsay, S. Identifying Single Bases in a DNA Oligomer with Electron Tunnelling. *Nat. Nanotechnol.* **2010**, *5*, 868–873.
53. Ohshiro, T.; Matsubara, K.; Tsutsui, M.; Furuhashi, M.; Taniguchi, M.; Kawai, T. Single-Molecule Electrical Random Resequencing of DNA and RNA. *Sci. Rep.* **2012**, *2*.
54. Phillips, J. C.; Braun, R.; Wang, W.; Gumbart, J.; Tajkhorshid, E.; Villa, E.; Chipot, C.; Skeel, R. D.; Kale, L.; Schulten, K. Scalable Molecular Dynamics with NAMD. *J. Comput. Chem.* **2005**, *26*, 1781–1802.
55. MacKerell, A. D., Jr.; Bashford, D.; Bellott, M.; Dunbrack, R. L., Jr.; Evanseck, J.; Field, M. J.; Fischer, S.; Gao, J.; Guo, H.; Ha, S.; *et al.* All-atom Empirical Potential for Molecular Modeling and Dynamics Studies of Proteins. *J. Phys. Chem. B* **1998**, *102*, 3586–3616.
56. Comer, J.; Dimitrov, V.; Zhao, Q.; Timp, G.; Aksimentiev, A. Microscopic Mechanics of Hairpin DNA Translocation through Synthetic Nanopores. *Biophys. J.* **2009**, *96*, 593–608.
57. Yoo, J.; Aksimentiev, A. Improved Parametrization of Li^+, Na^+, K^+, and Mg^{2+} Ions for All-Atom Molecular Dynamics Simulations of Nucleic Acid Systems. *J. Phys. Chem. Lett.* **2012**, *3*, 45–50.
58. Miyamoto, S.; Kollman, P. A. SETTLE: An Analytical Version of the SHAKE and RATTLE Algorithm for Rigid Water Molecules. *J. Comput. Chem.* **1992**, *13*, 952–962.
59. Andersen, H. Rattle: A "Velocity" Version of the Shake Algorithm for Molecular Dynamics Calculations. *J. Comput. Phys.* **1983**, *52*, 24–34.
60. Batcho, P. F.; Case, D. A.; Schlick, T. Optimized Particle-Mesh Ewald/Multiple-Time Step Integration for Molecular Dynamics Simulations. *J. Chem. Phys.* **2001**, *115*, 4003–4018.
61. Skeel, R.; Hardy, D.; Phillips, J. Correcting Mesh-Based Force Calculations to Conserve Both Energy and Momentum in Molecular Dynamics Simulations. *J. Comput. Phys.* **2007**, *225*, 1–5.
62. Humphrey, W.; Dalke, A.; Schulten, K. VMD: Visual Molecular Dynamics. *J. Mol. Graphics* **1996**, *14*, 33–38.
63. Wells, D. B.; Abramkina, V.; Aksimentiev, A. Exploring Transmembrane Transport through α-Hemolysin with Grid-Steered Molecular Dynamics. *J. Chem. Phys.* **2007**, *127*, 125101.
64. Brünger, A. T. X-PLOR, Version 3.1: A System for X-ray Crystallography and NMR. The Howard Hughes Medical Institute and Department of Molecular Biophysics and Biochemistry, Yale University, 1992.
65. Martyna, G. J.; Tobias, D. J.; Klein, M. L. Constant Pressure Molecular Dynamics Algorithms. *J. Chem. Phys.* **1994**, *101*, 4177–4189.
66. Aksimentiev, A.; Heng, J. B.; Timp, G.; Schulten, K. Microscopic Kinetics of DNA Translocation through Synthetic Nanopores. *Biophys. J.* **2004**, *87*, 2086–2097.
67. Isralewitz, B.; Izrailev, S.; Schulten, K. Binding Pathway of Retinal to Bacterio-Opsin: A Prediction by Molecular Dynamics Simulations. *Biophys. J.* **1997**, *73*, 2972–2979.
68. Koopman, E.; Lowe, C. Advantages of a Lowe-Andersen Thermostat in Molecular Dynamics Simulations. *J. Chem. Phys.* **2006**, *124*, 204103.